ACS AGRICULTURAL SCIENCE & TECHNOLOGY

pubs.acs.org/acsagscitech Article

Potential of Spatially Offset Raman Spectroscopy for Detection of Zebra Chip and Potato Virus Y Diseases of Potatoes (*Solanum tuberosum*)

Charles Farber, Lee Sanchez, Shankar Pant, Douglas Scheuring, Isabel Vales, Kranthi Mandadi,* and Dmitry Kurouski*

Cite This: *ACS Agric. Sci. Technol.* 2021, 1, 211−221 Read Online

ACCESS | Metrics & More | Article Recommendations | Supporting Information

ABSTRACT: Potato (*Solanum tuberosum* L.) is a staple food crop and part of an industry valued at an estimated $3.77 billion in the United States. Many varieties of potato are susceptible to zebra chip disease (ZC), a psyllid-vectored bacterial infection that renders the tubers unmarketable due to unappealing discoloration and taste. Similarly, potato virus Y (PVY) is a major pathogen of potatoes and other solanaceous crops that causes devastating damage to both foliage and tubers. These diseases are typically detected by enzyme-linked immunosorbent assay or polymerase chain reaction. ZC can also be diagnosed by a visual inspection of cut open tubers followed by frying to reveal the characteristic striping symptoms. However, these methods are invasive and destructive, as well as reagent, time, and labor consuming. Thus, quick and sample-general alternative methods for disease detection are highly desirable. In this proof-of-principle work, we demonstrate that spatially offset Raman spectroscopy (SORS) shows great potential for rapid and reagent-free detection of ZC or PVY diseases. Such detection is based on Raman identification of chemical changes in tubers associated with ZC or PVY. Chemometric analysis of spectra from intact potato tubers demonstrated over 90% accuracy of ZC detection. With data from cut open tubers, the prediction accuracy for ZC increased to over 90% for the prediction of PVY disease. We also show that potatoes from plants with either ZC or PVY diseases can be distinguished from each other and healthy tubers with approximately 95% accuracy. These results suggest that SORS has potential for noninvasive diagnostics of potato diseases.

KEYWORDS: *Candidatus Liberibacter solanacearum, CLso, disease diagnosis, Potato virus Y, Raman spectroscopy*

INTRODUCTION

Potato (*Solanum tuberosum* L.) is a major food crop, valued for its tubers, which store high amounts of starch.[1] Potatoes are grown around the world as a staple crop, as well as for snack foods such as french fries and potato chips.[2] In 2017, the United States produced $3.77 billion worth of tubers.[3] Potato derivatives have been developed for potential applications such as biodegradable packing materials and vehicle interiors.[4]

Potatoes are vulnerable to several pathogens including the Gram-negative bacterium *Candidatus* Liberibacter solanacearum (CLso). The bacterium is vectored by the potato psyllid *Bactericera cockerelli*, and causes zebra chip (ZC) disease, named for the characteristic discoloration of the tuber upon chipping and frying. Foliar symptoms include leaf scorch and curling, chlorosis, stunting, and swollen internodes. Importantly, ZC leads to decreased tuber yield and annual crop losses of US $33 million.[5] Although infected tubers are generally regarded as safe for human consumption, the alteration of flavor and unattractive brown discoloration, amplified by frying, renders them unmarketable for processed markets.[6] The amplification of discoloration by frying is often used for a diagnosis of this disease. However, it is laborious and impractical to randomly sample and fry to sort out all ZC-affected tubers during harvest or postharvest quality control. This means an infected potato may potentially go through quality control, thus decreasing the market quality of the produce. Polymerase chain reaction (PCR) diagnostics can offer sensitive detection of the bacterium in potato foliage or in its psyllid vector.[7−9] However, PCR would require many samples of plant material, is labor intensive, and consumes reagents. Additionally, PCR testing every potato plant or tuber for ZC in a field is highly impractical and, in the case of leaves, may lead to incorrect diagnosis due to an uneven distribution of the pathogen throughout its host.[6] To overcome these limitations, Liang and co-workers proposed to use near-infrared spectroscopy (NIR) for the detection of ZC, as well as the sugar content in intact potato tubers simultaneously.[10] Although Liang and co-workers showed that NIR provided an alternative to destructive PCR-based methods, it is unclear whether this method is disease specific and whether such analysis is reliable on more than one type/cultivar of potato.

In addition to ZC, potatoes are susceptible to many other diseases that can influence tuber composition. Potato virus Y (PVY) is a major viral pathogen of not only potatoes but also many other crops such as peppers, tomatoes, and tobacco.[11]

Received: January 25, 2021
Revised: March 23, 2021
Accepted: April 13, 2021
Published: April 26, 2021

Table 1. Summary of Potato Tubers Used in This Study

sample type	total number of tubers	healthy	infected	associated models (calibration)	notes
ZC Atlantic	16	8	8	At-CS, Bt-Var, Bt-CS, At-TB, At-SF, Ch-2D	infection status confirmed by PCR of leaf samples and frying of tubers from 8 biological replicates each (16 total plants)
ZC russets	14	7	7	Rs-CS, Bt-Var, Bt-CS	infection status confirmed by visual observation of symptoms; obtained from four different genotypes in the field
PVY chipping	5	3	2	Ch-PVY, Ch-2D	infection status confirmed by PVY-specific test strip

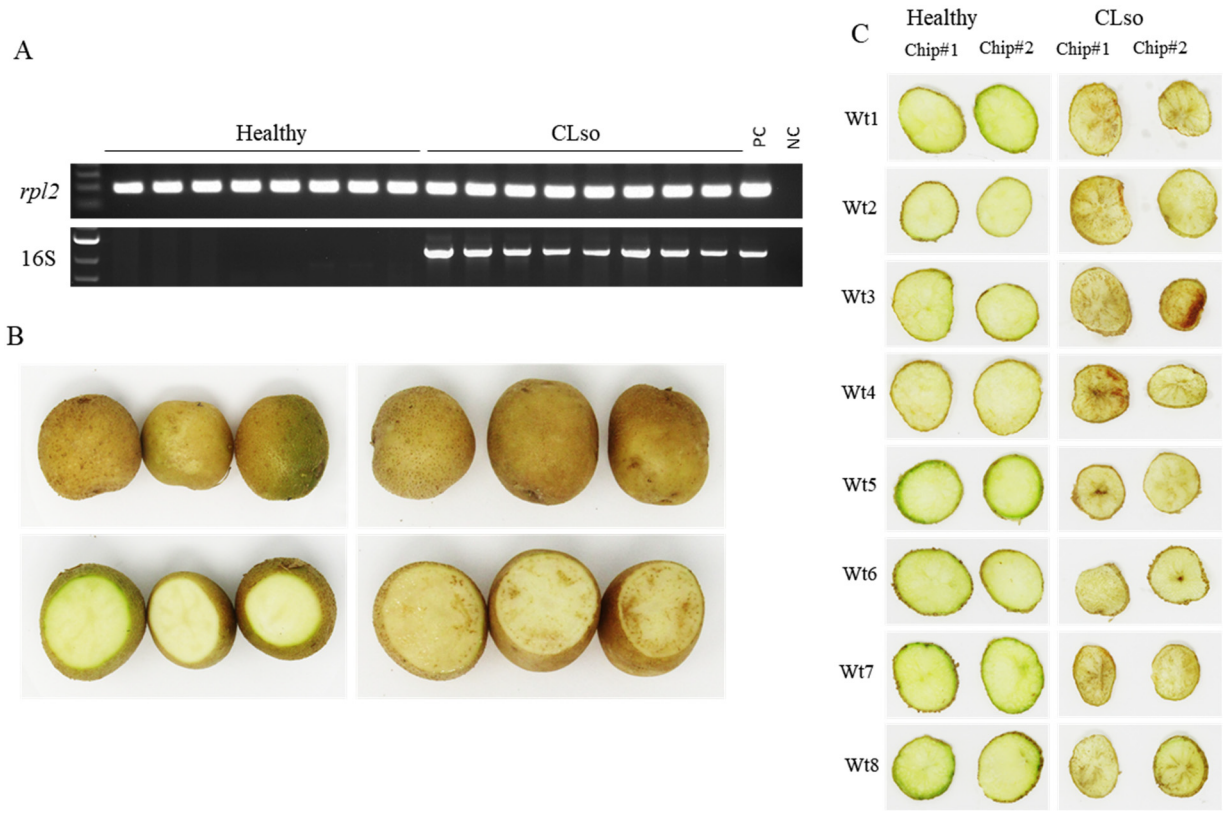

Figure 1. Identification of healthy and ZC potato using conventional PCR in leaf samples and chip frying assay with tubers. (A) Detection of *Candidatus* Liberibacter solanacearum (CLso) by conventional PCR in DNA extracted from leaves at 36 dpi. Upper and lower panels represent amplification of RPL2 of potato and 16S rDNA of CLso, respectively. PC, positive control; NC, negative control. (B) Typical ZC symptoms of brown discoloration in potato flesh as seen in cut-opened samples. No symptoms were observed in the healthy tubers (left). However, distinct brown spots (flecking) could be seen in CLso-infected tubers (right). (C) Fried slices of healthy (left) and CLso-infected potato tubers (right) were further used to determine ZC infection scores (Table S1).

The virus can be transferred vegetatively through seed tubers, as well as vectored by aphids. PVY disease symptoms are highly dependent on the strain and environment and can include both mosaicism in the leaves and necrotic lesions throughout the entire plant.[12] Like ZC, PVY detection could be achieved by both molecular and spectroscopic methods. For instance, Mehle and co-workers have demonstrated digital droplet PCR protocols for the detection of multiple different strains of PVY.[13] Recently, Griffel and co-authors used reflectance spectroscopy coupled to support vector machine (SVM) classification for PVY detection.[14] Couture and colleagues demonstrated that reflectance spectroscopy, in combination with advanced multivariate statistical methods, is capable of distinguishing potato plants by cultivar and PVY disease status.[15] These results demonstrate the potential of spectroscopic methods for disease detection. Expanding upon these findings, we investigated the potential of Raman spectroscopy as a fast, reagent-free method for the accurate detection of ZC and PVY diseases on potato.

Raman spectroscopy (RS) is a method based on the inelastic scattering of light that is used to probe sample chemical structure. The spectra generated from RS experiments are chemical fingerprints, specific to the analyzed sample. In many cases, the spectra from samples of different origins can be readily distinguished. In other cases, the variation between spectra can be subtle shifts in band position and/or intensity, requiring statistical methods, such as multivariate statistical analysis, to differentiate them. The potential of RS coupled with multivariate statistical analysis was previously demonstrated in many fields including forensics, art, and medicine.[16−18] Our group has demonstrated the potential of RS coupled with multivariate statistics for the detection of fungal, viral, and bacterial diseases on a broad spectrum of plants.[19−23] Specifically, we showed that RS could be used for the detection of *Candidatus* Liberibacter asiaticus that causes Huanglongbing, or citrus greening, on orange and grapefruit trees.[24,25] While Raman is quite powerful in detecting distinct chemical

https://doi.org/10.1021/acsagscitech.1c00024
ACS Agric. Sci. Technol. 2021, 1, 211−221

groups on a sample surface, its ability to probe deeper layers is limited.

By increasing the distance between the excitation and collection geometry, Raman signals can be obtained from deeper tissues within a sample. This analytical approach is known as spatially offset RS, or SORS.[26] SORS has been applied in noninvasive biomedical studies, as well as in national security projects.[27−29] We suspect that using only surface scans to detect disease-associated changes within the tuber would result in interference by the peel. Thus, we require a method to eliminate the spectral contribution of the peel. We hypothesize that by using SORS, we can capture the Raman spectra of potato tubers and differentiate metabolite changes associated with the healthy and diseased states, ultimately helping to diagnose ZC-diseased and PVY-infected tubers.

EXPERIMENTAL METHODS

Plant Materials − Overview. In this study, we used three different types of potato: the chipping-type "Atlantic" cultivar, a second chipping genotype, and four russet-type genotypes. Atlantic is the most widely planted public chipping potato variety in the US and was thus selected as an example of a chip-processing class potato. The Atlantic tubers used in this study have thin, light-brown peels. Russet-type potatoes can be marketed as fresh or processed and were therefore selected as a broader second category of potatoes. These potatoes have thicker, darker color peels than the Atlantic. We chose these types of potatoes to determine whether RS is limited by the physical properties of the sample. A brief overview of all tubers analyzed in this study can be found in Table 1.

Plant Materials and ZC Infections − Atlantic. Potato plants (cv. Atlantic) propagated in tissue culture media in Magenta vessels (Millipore Sigma) were transferred into potting soil in small pots (26.03 cm W × 22.35 cm H) to harden and were kept in growth chambers in insect-proof nylon mesh cages at 22 °C and a photoperiod of 14 h light/10 h dark for 2 weeks. After 2 weeks, the plants were transferred into 3.78 L pots for 3 weeks in growth chambers and subsequently planted in the field inside protected nylon mesh cages (125.4 cm × 125.4 cm) containing four plants in each cage. Eight plants were challenged with *Candidatus* Liberibacter solanacearum (CLso)-positive psyllids by exposing the lower most branches to 20 psyllids in a mesh bag (10 psyllids/bag/branch). Though four plants shared a cage, each plant was independently challenged with psyllids; thus, these eight plants are biological replicates. Psyllid bags were removed from challenged plants after 10 days. Eight healthy plants were simultaneously grown in two cages and were used as controls. Plants challenged with CLso-positive psyllids revealed the characteristic chlorosis and curling symptoms in leaves approximately 21 days post infestation (dpi). As expected, no visible symptoms of ZC were observed in plants that were nonchallenged. Newly emerging leaves (flush) were collected from eight healthy and psyllid infested plants at 36 days post infection (dpi) to determine the presence or absence of CLso by PCR diagnostics. Potato tubers were harvested at 60 dpi to determine CLso disease severity and determine tuber discoloration. Eight tubers from different plants were randomly selected from challenged and nonchallenged plants for ZC disease symptom diagnostics using chip frying assay (Figure 1A) and Raman spectroscopy analysis.

Insect Colonies and Maintenance. Potato psyllid (*Bactericera cockerelli*) harboring CLso (haplotype B) were reared on potato (var. Atlantic) plants in insect-proof cages (61 × 35 × 35 cm^3, BioQuip, Rancho Dominguez, CA) at 22.0 °C temperature and a photoperiod of 14 h light/10 h dark at Texas A&M AgriLife Research and Extension Center at Weslaco. The presence of CLso in the psyllids was confirmed by PCR as described below using genomic DNA extracted from psyllids, prior to using them for challenges.[9]

DNA Isolation and PCR Diagnostics. Total genomic DNA was extracted from leaf samples using a MagMAX total nucleic acid isolation kit (Applied Biosystems, Foster City, CA) according to the manufacturer's instruction with minor modifications as follow: ∼100 mg of leaf tissue was homogenized in 2 mL screw-cap microcentrifuge tubes for 40 s at 5000 rpm with a Precellys 24 homogenizer (MO BIO Laboratories, Carlsbad, CA) in the presence of two steel BB air gun beads (4.5 mm diameter) (Walmart Supercenter, Bentonville, AR). DNA was eluted with 85 μL of nuclease-free water and quantified by the concentration being measured using a NanoDrop 1000 spectrophotometer (Thermo Fisher Scientific, Wilmington, DE).

Polymerase chain reaction (PCR) was carried out to confirm the presence or absence of CLso in genomic leaf DNA from challenged and nonchallenged plants. The PCR reaction mix contained 12.5 μL of AccuStart II PCR ToughMix (2X), 1 μL of each primer (10 μM), 2 μL of DNA sample (100 ng), and 8.5 μL of nuclease-free water. The PCR amplification was performed in 1 cycle at 94 °C for 5 min, 37 cycles at 94 °C for 30 s, 68 °C for 30 s, and 72 °C for 1 min, and 1 cycle at 72 °C for 10 min, using a ProFlex PCR system (Applied Biosystems). OA2/OI2c primers (Jagoueix et al. 1996; Liefting et al. 2009) were used to amplify 16S rDNA (rDNA) sequences of CLso, and ribosomal protein L2 (RPL2) primers were used as an internal control to amplify the RPL2 endogenous gene of host plant as described previously (Table 2).[9,30−32] The DNA extracted from CLso-infected potato leaves were used as a positive control (PC), and water was used as a negative control (NC). PCR products were separated by electrophoresis on ethidium-bromide stained 1% agarose gel. The gel was visualized under UV light and photographed using a GelDoc-ItTS3 imager (UVP, LLC, Upland, CA).

Table 2. Sequences of Primers Used in This Study to Detect the Presence of CLso Bacteria in Potato Leaves

gene		sequence
CLso 16S rDNA	forward	5′-GCGCTTATTTTTAATAGGAGCGGCA-3′
	reverse	5′- GCCTCGCGACTTCGCAACCCAT-3′
rpl2	forward	5′-GAGGGCGTACTGAGAAACCA-3′
	reverse	5′-CTTTTGTCCAGGAGGTGCAT-3′

Plant Materials − russet ZC and Potato Virus Y. Four russet genotypes (COTX15271-1Ru, OR12133-10, COTX14132-1Ru, and COTX04303-3Ru) were grown in Dalhart, TX using standard agronomic management practices for commercial potatoes in the region. The four genotypes are experimental lines and thus do not yet have defined market (fresh or processed) classes. They were planted in May and harvested in September. Potato tubers were cut in half and inspected for ZC symptoms. The level of ZC incidence under natural field conditions was low (0.5%); however, tubers with ZC symptoms were identified. Healthy and diseased tubers (with ZC symptoms) of the four genotypes were collected, suberized, and stored at room temperature until examination by RS in November.

Infected and noninfected chipping potatoes tubers (genotype TX12484-2W) were planted by the end of August 2019 and grown under greenhouse conditions in the Horticulture Department building at Texas A&M University, College Station, TX. The PVY status was confirmed in the leaves using an Agdia ImmunoStrip for Potato virus Y in November 2019. The strain of PVY was not determined, but no necrosis was observed in the tubers. Tubers from infected and noninfected plants were collected soon after and examined by RS in November.

Raman Spectroscopy and Statistics − Overview. We first investigated whether RS could detect ZC-associated changes in one market class of potato (Atlantic chipping), both by spectral analysis and by statistical modeling (At-CS). We then checked whether the At-CS model could be used to predict the ZC status of another market class of potato (russet-type). In parallel, we built a new model (Rs-CS) using only the russet-type potatoes and used this model to predict the ZC status of the Atlantic potatoes. We also developed a separate model (Bt-Var) to investigate whether RS could be used to predict the market class of healthy potatoes, as well as a model (Bt-CS) that combined both market classes to distinguish between

https://doi.org/10.1021/acsagscitech.1c00024
ACS Agric. Sci. Technol. 2021, 1, 211−221

Table 3. Summary of PLS-DA Models Built for This Study.[a]

model name	spectra used	groups compared	number of spectra	LVs	% LV 1	% LV 2	% LV 3	average TPR (%)	MCC
At-CS	Atlantic cut surface	Atl. healthy vs ZC	29/13	3	40	12.8	20.08	100	1.000
Rs-CS	russet-type cut surface	Rus. healthy vs ZC	42/42	12	40.85	11.88	19.81	92.5	0.858
Bt-Var	healthy Atlantic and russet-type	Atl. vs Rus.	42/29	6	47.67	11.52	24.05	100	1.000
Bt-CS	Atlantic and russet-type: all ZC data set	healthy Atl and Rus. vs ZC	71/54	11	40.72	11.06	14.8	92.3	0.855
Ch-PVY	chipping PVY healthy and infected	Ch. healthy vs PVY	14/9	8	34.32	32.79	13.81	94.5	0.911
Ch-2D	Atlantic and chipping healthy, chipping PVY, and Atlantic ZC	Atl. healthy vs PVY vs ZC	43/10/13	8	32.58	19.31	14.6	95	n/a
At-TB	Atlantic through peel	Atl. healthy vs ZC	48/48	8	22.25	33.16	18.15	93.5	0.898
At-SF	Atlantic surface	Atl. healthy vs ZC	48/48	4	10.02	13.43	19.97	72.5	0.465

[a]Number of spectra, Class 1/Class 2/Class 3...; LV, latent variable; % LV *X*, percentage of variation explained LV *X*; TPR, true positive rate; MCC, Matthews correlation coefficient. Ch2D n/a in the MCC column: MCC is a measure of binary model performance and was thus not calculated for a model with three classes.

healthy and infected tubers of either market class. Additionally, we demonstrated that RS could detect Potato virus Y in the chipping class tubers (Ch-PVY). We then showed that this method can differentiate healthy and ZC- and PVY-infected tubers within the chipping class (Ch-2D). Finally, we demonstrated that SORS is necessary for the detection of ZC symptoms in Atlantic tubers by comparing models assembled from data acquired with the SORS (At-TB) and surface-scanning (At-SF) modes of the portable device.

Raman Spectroscopy. All spectra were collected with an Agilent-Cobalt Resolve SORS instrument equipped with an 830 nm laser source and a spectral resolution of 15 cm^{-1}. Data were acquired in the "through barrier" setting from potatoes under two different conditions: directly from exposed interior tissues (tuber cut in half; "cut surface") and through the fully intact peel ("through peel"). The spectra were automatically baselined by the instrument software. For the cut surface tissue scans, an offset of 1 mm, a 2 s integration time, and 15 accumulations were used. Spectra acquired through the peel of the potato were collected with the following parameters: For the surface scans, 495 mW power, no offset, 1 s integration time, and 1 accumulation were used. For the through barrier scans, 495 mW power, an offset of 2 mm, a 2 s integration time, and 30 accumulations were used. The instrument then automatically conducted a scaled subtraction of the surface spectra from the offset spectra to generate SOR spectra. We opted to report nonsubtracted offset spectra (subsequently referred to as "offset spectra") for our exposed interior tissue analysis. The surface scan in this case represents the outer layer of interior potato tissue and should be similar to the inner layers of tissue. For through peel analysis, reducing the contribution of the potato peel to our spectra is essential for statistical model performance; therefore, we chose to report the SOR spectra that have the peel contribution subtracted away.

For all figures, spectra were normalized to 1460 cm^{-1}. The band at 1460 cm^{-1} was selected because it corresponded to CH_2 vibrations that are common in biological molecules. Therefore, we used it as an internal standard. Spectra presented in the paper are also not mean-centered to maintain readability.

Statistics. Spectra were imported into Matlab for analysis in the addon PLS_Toolbox (eigenvector Research Inc.). To classify our spectral data, we chose partial-least squares discriminant analysis (PLS-DA). PLS-DA is based on regular PLS, which is typically used in linear regression. PLS typically includes quantitative explanatory and response variables, whereas PLS-DA has quantitative explanatory and qualitative response variables. These qualitative response variables are known as classes.[33] In this study, our quantitative explanatory variables are our Raman spectra, which have their own explanatory (Raman shift) and response (intensity) variables. The qualitative response variables are the health statuses of the potatoes that we collected spectra from.[33]

PLS-DA is not the only method for building classifying models based on known classes. One example is SIMCA, which is based on principle component analysis. In our experience, as well as from other groups, PLS-DA works better than SIMCA for Raman data classification. Another method is known as linear discriminant analysis (LDA). While LDA typically performs well, it has issues with data where many of the explanatory variables have linear relationships with each other. This trend, known as multicollinearity, is common in Raman spectra: the intensities of Raman bands near each other in the spectrum, such as 1002 and 1005 cm^{-1}, tend to have linear relationships. PLS-DA, in contrast, works well with multicollinear data.[34,35] On the basis of these advantages over other methods and our experience, we have chosen PLS-DA as our classification method.

The spectra were normalized with standard normal variate scaling (SNV) and mean-centered before use in model-building. The model was then trained using the spectral data with classes assigned based on the health status of the source potato tuber. Following this, the software performed a cross-validation, where the order of the data is shuffled (classes are maintained), portions of the data set are excluded, and the rest is used to rebuild the model. The model then attempts to classify the excluded spectra. We report cross-validated results to demonstrate that the model should be capable of classifying data it has never seen before. Only cross-validation results are reported because our potato sample size, and subsequently, our spectral sample sizes, were small, limiting our ability to separate the data into calibration and validation sets without compromising model performance. All reported models were found to be significant (α = 0.05) using 100 iterations of the permutation test unless stated otherwise.[36,37] The permutation test determines the significance of the classes of a classification model by randomly and repeatedly reassigning data to different categories and then building new models. If the groupings are significant, models built from randomly classified data should perform poorly.

The models were evaluated on the grounds of permutation test performance and Matthews correlation coefficient (MCC) scores. MCC is a measure of binary model prediction performance.[38] A MCC value closer to positive 1 indicates a stronger performance. For the three-group model (Ch-2D), the permutation test and average true-positive rate (TPR) were used in its evaluation. A summary of all models reported in this study can be found in Table 3.

ANOVA (analysis of variance) tests were conducted to determine whether the intensities of selected Raman bands were significantly different across the classes. The 1460-normalized intensities of the bands of interest were used for these analyses. ANOVAs were run

https://doi.org/10.1021/acsagscitech.1c00024
ACS Agric. Sci. Technol. 2021, 1, 211−221

using the anova1 function in MATLAB. Raman bands that showed significant differences in the ANOVA were then tested with the Tukey HSD *post hoc* test to determine which groups were significantly different from each other using the multicompare function. The ANOVA results are summarized in Table 4 and Figure S1.

Table 4. Summary of ANOVA and Tukey HSD Results on All Raman Bands for the Ch-2D Combined Dataset[a]

band (cm^{-1})	group relation
441	c ≪ ab
479	c ≪ ab
523	NSD
578	NSD
615	NSD
717	NSD
768	NSD
865	c ≪ b
940	c ≪ ab
1007	c ≪ ab
1054	c ≪ ab
1084	c ≪ ab
1126	c ≪ ab
1153	c ≪ a ≪ b
1208	ab ≪ c
1261	a ≪ c
1340	c ≪ a
1383	c ≪ a
1398	c ≪ a
1460	NSD
1530	a ≪ b
1600	a ≪ bc
1633	a ≪ b

[a]NSD, ANOVA indicated no significant differences ($p > 0.05$). ≪, ANOVA indicated that a significant difference existed ($p < 0.05$) and the grouping(s) on the left of the ≪ were found to be significantly less intense than those on the right by Tukey HSD *post hoc* testing ($p < 0.05$). a, healthy; b, PVY; c, ZC.

RESULTS

PCR and Visual Confirmation of ZC in Atlantic Tubers. The chipping of tuber samples collected from CLso-positive plants displayed brown vascular discoloration/necrotic spots or flecking, a typical symptom of ZC; however, tubers from nonchallenged plants did not show the vascular discoloration (Figure 1B). Further chip frying revealed vascular tissue discoloration in all the tubers from the plants exposed to CLso-positive psyllids with ZC scores ranging from 1 to 3. However, no vascular discoloration was observed (ZC scales = 0) for all tubers collected from nonchallenged plants (Figure 1C and Table S1).[39]

Assessment of Spectra Taken from the Exposed Potato Interior Tissues. First, we acquired spectra from the exposed Atlantic tuber interior tissues. We discovered that the infected tubers had lower intensity Raman spectra compared to the healthy potatoes. A likely explanation for this is that the ZC-associated tuber discoloration, biochemical changes, and necrotic areas influence spectra collection and intensity. Because the discolored potato tissue is slightly darker, it may scatter fewer photons than the lighter colored healthy tissue. In this case, we cannot use these spectra without further processing. To further improve a spectral comparison between the healthy and infected potatoes, we normalized the data to the 1460 cm^{-1} band (Figure 2A). This band, assigned to CH_2, was selected to limit the bias toward specific classes of molecules introduced through normalization. Vibrational band assignments were made on the basis of previously reported spectroscopic analyses of carbohydrates, protein, carotenoids, and polyphenols (Table 5).[40−52] We believe that most of these bands are likely associated with carbohydrates. To confirm this, we obtained the Raman spectra of powdered pectin and amylopectin (Figure S2)

We found that, in the normalized spectra, most spectral bands remained less intense in the spectra of infected potatoes than in those from healthy tubers, suggesting quantitative differences in analytes between the infected and healthy tubers. Only the bands at 1208, 1261, and 1600 cm^{-1} did not follow this trend; these are more intense in the infected spectra than the healthy spectra.

Next, we asked whether coupling exposed interior tissue Raman spectra to multivariate statistical analysis could enable the prediction of ZC status in these Atlantic tubers. In total, 45 offset spectra were used to build and cross-validate the resulting model, Atlantic-cut surface (At-CS). This model enabled 100% accurate differentiation of healthy and ZC-infected Atlantic tubers from interior tissue spectra alone. The model was used to generate a loadings plot (Figure S3). Loadings plots show what portions of the spectrum were the most important for the model to make its predictions. These results demonstrate that RS can be used to predict the ZC status of cut Atlantic tubers.

One may question whether this spectroscopic method is specific to different market classes of potato. To answer this question, we acquired spectra from healthy and ZC-infected russet-type tubers (Figure 2B). At-CS was then used to classify the russet-type spectra to determine the ZC status and was found to perform quite poorly (Table 6). These results suggest that a Raman-based approach for ZC diagnostics must be calibrated for each type and possibly each variety of potatoes. Therefore, we built and cross-validated a new model using russet-type spectra from the exposed tissue (Rs-CS) (Figure S4). Rs-CS was about 90% accurate in predicting disease status in russet-type tubers. We then further confirmed the market class specificity of PLS-DA by attempting to predict the Atlantic ZC status using Rs-CS, which performed as poorly as its complement (At-CS) (Table 7). These results suggest that PLS-DA models built based on only one variety of potato are specific only for that variety. This is in good agreement with Gold and colleagues, who demonstrated the potato cultivar dependence of disease detection in reflectance spectroscopy.[53]

We then questioned whether RS could be used to differentiate tubers by market class. To further demonstrate that the Atlantic and russet-type tubers are spectroscopically distinct, we built and cross-validated a model (Bt-Var) using only spectra from healthy tubers from the ZC data sets to differentiate between the classes (Figure 2C). Bt-Var reports 100% accurate differentiation of the two classes (Figure S5). These results demonstrate that, in addition to ZC diagnostics, RS has a potential for the determination of the potato market class. These results confirm our recent findings that RS could be used for the identification of potato varieties based on their spectroscopic signatures.[23]

On the basis of the good performance of three PLS-DA models (At-CS, Rs-CS, and Bt-Var), we sought to determine whether different market classes of potato could be combined to make general predictions of ZC infection. To demonstrate

https://doi.org/10.1021/acsagscitech.1c00024
ACS Agric. Sci. Technol. 2021, 1, 211−221

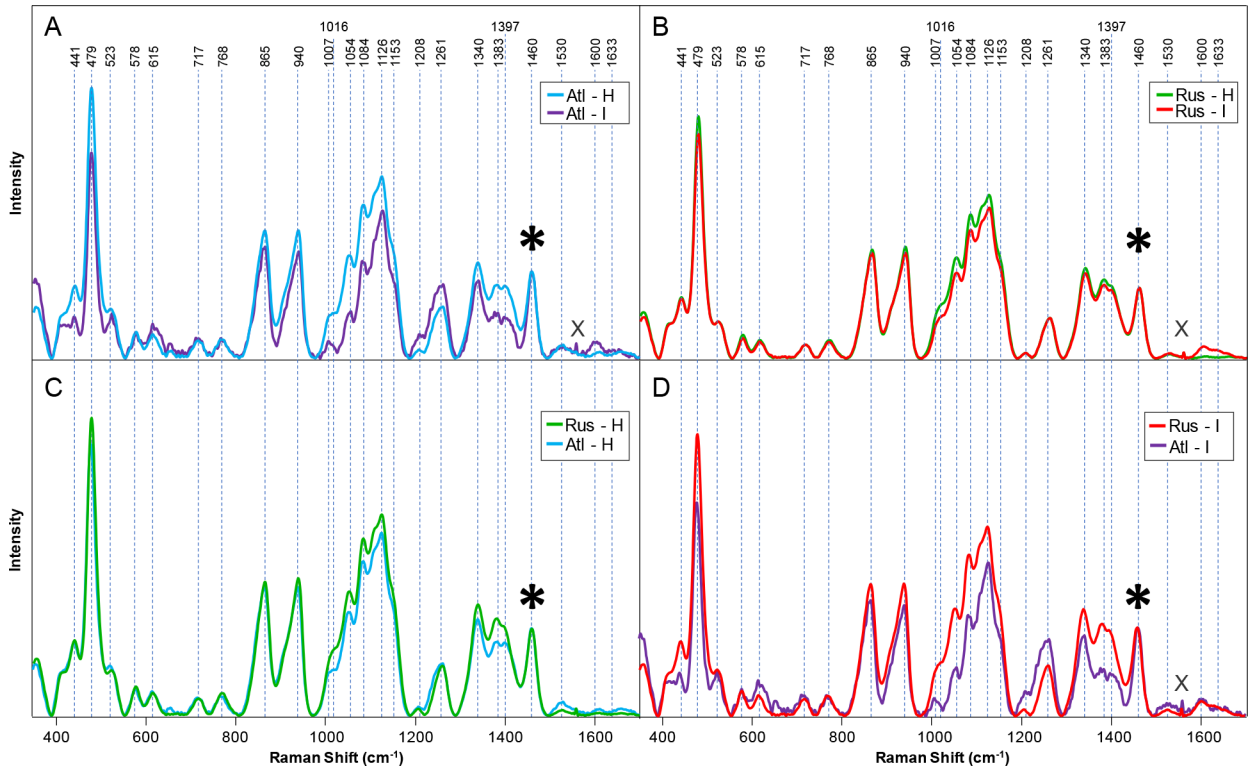

Figure 2. Averaged normalized offset spectra of potato interior tissue for the ZC data set. Spectral variations in each quadrant can potentially be explained chemical changes associated with (A and B) infection or (C and D) genetic background. These comparisons reveal that not only do the healthy and infected tubers have differing chemical compositions but also ZC-associated changes to the tuber may depend on the type of potato infected. (A) Atlantic (Atl) healthy and infected; (B) russet-type (Rus) healthy and infected; (C) russet-types and Atlantic healthy; (D) russet-types and Atlantic infected. H, healthy; I, infected with ZC; *, normalization band (1460 cm^{-1}); X, instrument artifact spike.

Table 5. Vibrational Band Assignments for Potato Spectra

band (cm^{-1})	vibrational mode	assignment
441	skeletal modes of pyranose ring	carbohydrates[61,62]
479	C—C—O and C—C—C deformations; related to glycosidic ring skeletal deformations	carbohydrates[61]
	δ(C—C—C) + τ(C—O) scissoring of C—C—C and out-of-plane bending of C—O	
523	δ(C—C—O) + τ(C—O) of carbohydrates	carbohydrates[61]
578	ν(C—O) + ν(C—C) + δ(C—O—H)	cellulose, phenylproanoids[63]
615	δ(C—C—O) of carbohydrates	carbohydrates[61]
717	δ(C—C—O) related to glycosidic ring skeletal deformations	carbohydrates[61]
768	δ(C—C—O)	carbohydrates[61]
865	δ(C—C—H) + δ(C—O—C) glycosidic bond; anomeric region	carbohydrates[61]
940	skeletal modes; δ(C—O—C) + δ(C—O—H) + ν(C—O) α-1,4 glycosidic linkages	carbohydrates[64]
1007	in-plane CH_3 rocking + C—C	carotenoids[44]
1054	ν(C—O) + ν(C—C) + δ(C—O—H)	carbohydrates[61]
1084	ν(C—O) + ν(C—C) + δ(C—O—H)	carbohydrates[61]
1126	ν(C—O) + ν(C—C) + δ(C—O—H)	carbohydrates[61]
1153	ν(C—O—C), ν(C—C) in glycosidic linkage, asymmetric ring breathing	carbohydrates[65]
1208	aromatic ring modes of phenylalanine and tyrosine; symmetric O—CH_3 wag + C—O—H bending	proteins,[66] phenylpropanoids[67]
1261	δ(C—C—H) + δ(O—C—H) + δ(C—O—H)	carbohydrates[48,61]
1340	ν(C—O); δ(C—O—H)	carbohydrates[61]
1383	δ(C—O—H): coupling of the CCH and COH deformation modes	carbohydrates[61]
1398	δ(C—C—H)	carbohydrates[61]
1460	δ(CH) + δ(CH_2) + δ(C—O—H) CH, CH_2, and COH deformations.	aliphatic[61]
1530	-C=C-	carotenoids[49]
1600	ν(C—C) aromatic ring + σ(CH)	phenylpropanoids,[50,68] proteins,[66]
1633	C=C—C(ring)	phenylpropanoids[52]

that RS can detect ZC status regardless of market class, we built and cross-validated a model (Bt-CS) using both the russet-type and Atlantic tuber spectra (Figure S6). This cross-class ZC model was about 92.3% accurate in determining disease status. With these four models, we demonstrated that RS coupled to PLS-DA can predict not only the disease status

https://doi.org/10.1021/acsagscitech.1c00024
ACS Agric. Sci. Technol. 2021, 1, 211−221

Table 6. Confusion Matrix for Prediction of Russet-Type Potato ZC Status by the Atlantic ZC Model (At-CS)[a]

	healthy	infected
healthy	40	40
infected	2	6
MCC	0.162	

[a]MCC: Matthews correlation coefficient.

Table 7. Confusion Matrix for Prediction of Atlantic Potato ZC Status by the Russet-Type ZC Model (Rs-CS)[a]

	healthy	infected
healthy	29	5
infected	0	8
MCC	0.724	

[a]MCC: Matthews correlation coefficient.

but also market class of potatoes with high accuracy. One may expect that a relatively poor performance of this model could be due to genetic differences between potato varieties. Thus, as was discussed above, market class specific models rather than generic models should be used for Raman-based ZC diagnostics.

We then questioned whether RS could detect other potato diseases. We acquired spectra from young chipping tubers grown under greenhouse conditions harvested from plants that tested positive for PVY (Figure 3). We identified four bands,

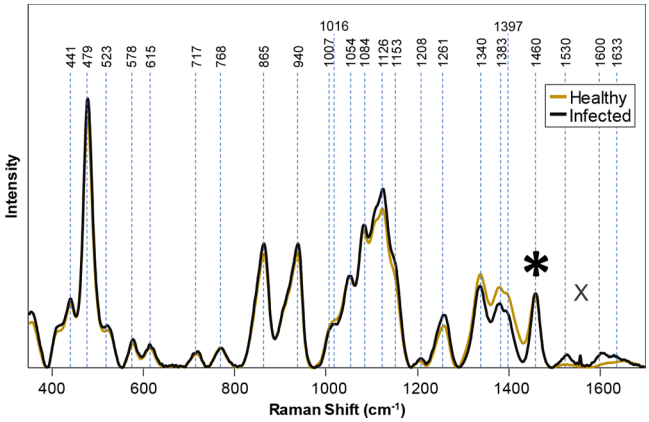

Figure 3. Averaged normalized offset spectra of healthy and PVY-infected chipping potatoes acquired from the exposed interior tissue. The differences between the healthy and infected spectra can potentially be explained by the health status of the tuber. *, normalization band (1460 cm^{-1}); X, artifact spike.

1153, 1530, 1600, and 1633 cm^{-1}, that showed significant differences in intensity between the spectra from tubers of healthy and PVY-positive plants (Table 4). We found that the 1153 cm^{-1} differed significantly across the healthy, ZC, and PVY classes (Figure 4). We then built a model (Ch-PVY) to differentiate between the diseased and healthy tuber spectra (Figure S7). This model was about 94.5% accurate in this classification. This result suggests Raman can be used for the accurate detection of two different potato diseases. One may question whether this Raman method is disease specific. Using the Atlantic ZC and the chipping PVY data sets, we calibrated a new model (Ch-2D) to differentiate between healthy, ZC-infected, and PVY-infected potatoes (Figure S8). We found

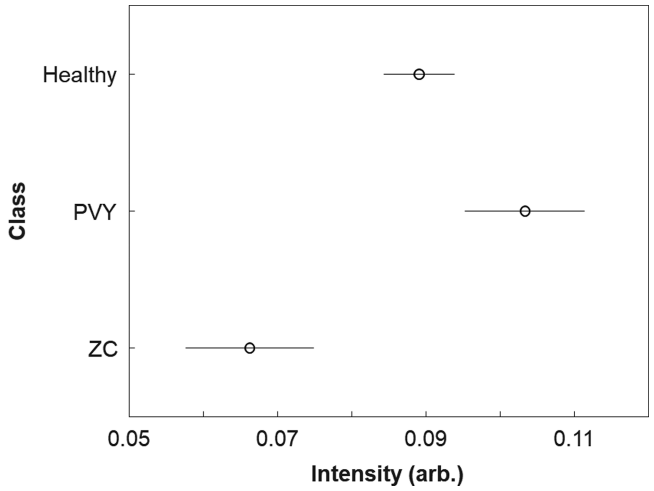

Figure 4. 95% confidence intervals for the true mean 1460 normalized intensities of the 1153 cm^{-1} band in the spectra of tubers from healthy, ZC-infected, and PVY-infected plants.

that this model was on average 95% accurate for differentiating these three groups, indicating that Raman may offer disease-specific detection. Further studies with additional pathogens will be required to fully demonstrate disease specificity.

Assessment of Spectra Taken through Intact Peel. To enable noninvasive diagnostics, we conducted measurements through the intact peel of the Atlantic potatoes to determine whether we could detect chemical changes associated with ZC without slicing the potato tuber (Figure 5A). In these spectra, the 1600 and 1633 cm^{-1} bands became more apparent. We were unable to obtain quality spectra from russet-type potatoes through their peels. This may have to do with the characteristics of the russet-type peel, such as thickness and color, as well as the age of samples.

We then sought to determine whether multivariate statistical analysis of these spectra could be used to predict the ZC status of intact Atlantic tubers. Our model, At-TB, was built using 96 SOR spectra acquired from Atlantic tubers through their peels (Figure S9). At-TB was 93.5% accurate in the cross-validation of these spectra. This result demonstrates the potential of SORS for the noninvasive analysis of potato tubers.

We wanted to confirm that SORS was required to detect ZC through the peel of the potato. To do this, we built a model (At-SF) using the surface scans (Figure 5B) acquired from the intact potatoes. At-SF was 72.5% accurate in cross-validation with the spectra. Additionally, this model was found to be not significant by permutation testing. Thus, SORS greatly improves ZC diagnostics in intact potato tubers compared to RS.

DISCUSSION

The vibrational bands in the spectra collected from potato tissue can be primarily assigned to carbohydrates, carotenoids, and phenylpropanoids (Table 5). Carbohydrates are associated with the following bands in the Raman spectra of potatoes: 441, 479, 523, 578, 615, 717, 768, 865, 940, 1054, 1084, 1126, 1153, 1261, 1340, 1383, and 1398 cm^{-1}. These likely correspond to starch and other carbohydrates, with starch being the major nonwater (solid) component of potato tissue.[1] To support this hypothesis, we collected Raman spectra of pure amylose and amylopectin, which appeared very similar to the potato spectra (Figure S2). As described before, even after

https://doi.org/10.1021/acsagscitech.1c00024
ACS Agric. Sci. Technol. 2021, 1, 211−221

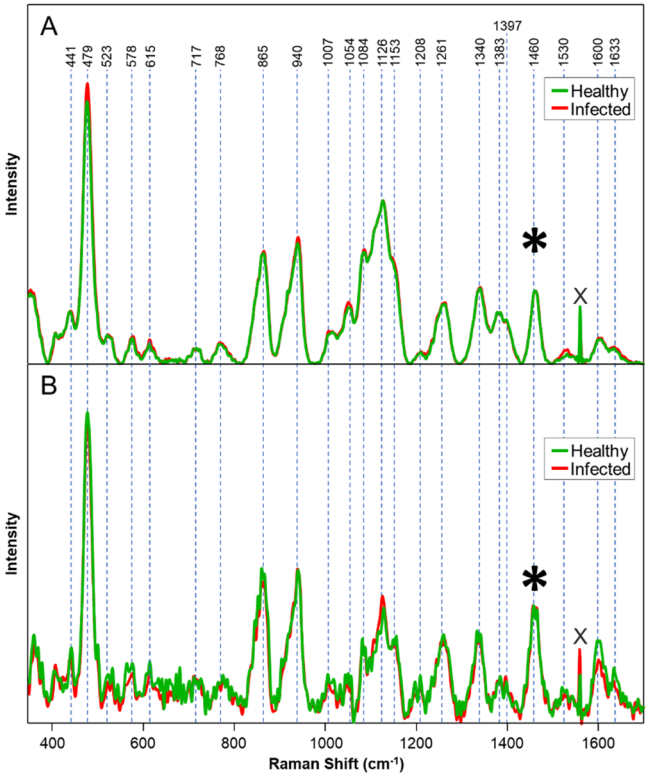

Figure 5. Averaged normalized (A) spatially offset Raman (SOR) and (B) surface spectra from healthy or ZC-infected intact Atlantic potato tubers. Differences in spectral quality can be explained by differences in acquisition parameters as well as poor scattering efficiency by the potato peel. The SOR scan shows clearly resolved bands, whereas, in the surface scans, many bands cannot be resolved due to the increased noise. *, normalization band (1460 cm^{-1}); X, artifact spike.

normalization, the intensities of the carbohydrate-associated Raman bands were lower in the infected spectra than the healthy spectra. As Raman intensities are closely associated with the concentration of analyte, this suggests that the total starch and carbohydrate content of the tuber may decrease following infection. These changes indicate that RS may be able to detect changes in the carbohydrate profile of tubers under disease-associated stress conditions. Our observation is in line with previously reported results from Buchman and colleagues, who estimated starch content by measuring specific gravity.[54] They showed that reducing sugars increase in concentration following CLso infection. One may hypothesize that the changes in the Raman spectrum maybe associated with these sugars. However, further testing by mass spectrometry would be required to determine the exact identities of sugars changing in the tuber, which is beyond the scope of the present work.

Carotenoids can be associated with the slight yellow coloration of the potato tissue in some cultivars.[55] In the Raman spectra of potatoes, the bands at 1007, 1153, and 1530 cm^{-1} likely correspond to carotenoids and associated molecules. The decreases in intensity in the bands in the infected spectra may suggest that ZC disease may be associated with decreases in potato carotenoid content.

Phenylpropanoids are a family of branched polyphenolic polymers, including suberin and lignin, that are associated with toughening of the cell wall.[56,57] The aromatic moieties of these polymers may be associated with bands at 1208 and 1600 cm^{-1}. The intensity of the 1600 cm^{-1} significantly increased in both the ZC- and PVY-infected spectra relative to the healthy ones, suggesting that the concentration of the phenylpropanoids and other aromatics has increased. This observation is in good agreement with Singh and colleagues, who observed an increase in the phenylpropanoid content of ZC tubers using the gallic acid equivalence method.[58] Overall, our results suggest that RS can reliably detect the characteristic metabolite changes associated with ZC or PVY infection in potato plants.

The loadings plots (Figures S3−S9) reveal which spectral regions the model determined to be the most important for classifying the data. Stronger bands, in the positive or negative direction, indicate greater importance. In many of the loadings plots, broad bands across 400−500, 1000−1200, and 1300−1500 cm^{-1} are present. As described previously, the bands in these regions are associated with carbohydrates, which would be logical for ZC detection. In the loadings plots for Rs-CS (Figure S4), a broad band over 1600−1650 cm^{-1}, where the previously assigned phenylpropanoid bands appear, is present. Its low importance in the At-CS loadings (Figure S3) may suggest differences in how the CLso interacts with different market classes of potato. A similar pattern was observed in the Ch-PVY loadings plot (Figure S7). The loadings plot for Bt-Var (Figure S5) reveals that differences associated with carbohydrates are the most significant for classification. The loadings plots of Ch-2D (Figure S8) appear to have features of both the At-ZC and Ch-PVY plots, which is reasonable as data from At-ZC and Ch-PVY was used in the construction of Ch-2D. This indicates that the individual features associated with differentiation of spectra obtained from healthy tubers and diseased tubers are also important for the differentiation of these diseases from each other. The loadings plots suggest that, for the detection of either these diseases, changes in carbohydrate-associated bands are the most important, while phenylpropanoid-associated band importance depends on market class and infection. Additionally, carbohydrates are the most important factor for differentiating the russet-type and Atlantic potatoes.

We have demonstrated that the spectra acquired from the russet-type and Atlantic potatoes differ from each other. We used our ZC-identifying models built with one class (At-CS and Rs-CS) to attempt assigning disease status for the other and found the resulting prediction to be poor (Tables 6 and 7). It is well-known that different market classes have differing nutrient content and physical properties, both of which can greatly influence Raman spectra,[59] so this result was expected.

This result is also in line with experimental evidence recently reported by Morey and colleagues. The researchers showed that, by using Raman and chemometric analyses, potatoes of different genotypes could be distinguished with high accuracy.[23] They also demonstrated that potatoes of the same cultivar grown around 140 miles away from each other (Springlake, TX and Dalhart, TX) could be differentiated. It has yet to be determined whether the location itself or differences in stresses experienced during growth dominate in the determination of this differentiation. The success of the combined Bt-CS model for determining ZC status in both Atlantics and russet potatoes suggests that the differences across market classes, genotype, or location may be smaller than those of biotic stress. Additional studies will be required to explore the significance of plant location and stresses on acquired Raman spectra.

https://doi.org/10.1021/acsagscitech.1c00024
ACS Agric. Sci. Technol. 2021, 1, 211−221

In the through peel spectra, few major spectral changes were observed (Figure 5A). The previously noted 1633 cm^{-1} band, associated with the double-bond stretches of aromatic rings, is only visible in these SOR spectra. Suberin, which contains a large polyaromatic domain assembled from phenylpropanoids, is a major component of the potato outer peel, so this is reasonable as the spectra were acquired through the peel.[60] In the exposed potato tissue readings, the peel is not in the way, so these bands have much lower intensities. We found that the loadings plot of At-TB (Figure S7) was quite distinct from that of At-CS. This may have to do with variations in the spectrum associated with probing the tissue at the center of the tuber versus at the periphery.

As described in our results, we observed that through peel analysis is limited to certain types of potato, such as Atlantic, that have thinner and/or lighter color peels. This analysis proved to be impractical for the russet types. It is possible that the further optimization of collection parameters or different instrumentation may prove capable of russet-type through peel analysis. Additionally, one can envision that removing (peeling) a small piece of peel or excoriating the peel before scanning may enable minimally invasive SOR analysis of these tubers. However, for the types of potatoes studied, cutting open the potato resulted in higher accuracy classification models. Additionally, Raman spectra can be acquired within seconds, enabling extremely fast disease detection.

We believe that SORS could be a useful alternative to reagent-based methods such as PCR. Recently, it was demonstrated that RS is capable of detecting citrus greening disease several months before the causative bacterium is detectable by qPCR.[25] This result demonstrates that RS is capable of supplementing more established methods. In general, one can envision using SORS and calibrated statistical models to perform a quick initial disease screen of plant samples. Because the SORS method is nondestructive, these samples could still be analyzed by PCR, ELISA, or other traditional methods if a secondary validation is desired. We believe that SORS/RS will ultimately coexist with the existing methods, providing a first initial screen in less characterized systems, while potentially replacing these methods when the system is heavily characterized in RS.

Although destructive in some cases, SORS can enable high-accuracy disease detection in potato tubers, serving as a fast alternative to traditional detection methods. These results suggest that a hand-held Raman spectrometer shows great potential to be multifunctional tool in agriculture, i.e., determining disease status, nutrient content, and/or verify genetic backgrounds simultaneously.

■ ASSOCIATED CONTENT

Supporting Information

The Supporting Information is available free of charge at https://pubs.acs.org/doi/10.1021/acsagscitech.1c00024.

Figures of 95% confidence intervals, Raman spectra, and loadings plots and table of ZC severity of Atlantic potatoes scanned in this study from the Atlantic ZC dataset (PDF)

■ AUTHOR INFORMATION

Corresponding Authors

Kranthi Mandadi − *Texas A&M AgriLife Research and Extension Center at Weslaco, Weslaco, Texas 78596, United States; Department of Plant Pathology and Microbiology, Texas A&M University, College Station, Texas 77843, United States*; Email: kkmandadi@tamu.edu

Dmitry Kurouski − *Department of Biochemistry and Biophysics, Texas A&M University, College Station, Texas 77843, United States; The Institute for Quantum Science and Engineering, Texas A&M University, College Station, Texas 77843, United States*; orcid.org/0000-0002-6040-4213; Email: dkurouski@tamu.edu

Authors

Charles Farber − *Department of Biochemistry and Biophysics, Texas A&M University, College Station, Texas 77843, United States*

Lee Sanchez − *Department of Biochemistry and Biophysics, Texas A&M University, College Station, Texas 77843, United States*

Shankar Pant − *Texas A&M AgriLife Research and Extension Center at Weslaco, Weslaco, Texas 78596, United States*

Douglas Scheuring − *Department of Horticultural Sciences, Texas A&M University, College Station, Texas 77843, United States*

Isabel Vales − *Department of Horticultural Sciences, Texas A&M University, College Station, Texas 77843, United States*

Complete contact information is available at: https://pubs.acs.org/10.1021/acsagscitech.1c00024

Funding

Funding for the study was provided by the Governor's University Research Initiative (GURI) grant program of Texas A&M, GURI Grant Agreement No. 12-2016, M1700437 to D.K. and TexasA&M AgriLife Research Insect-Vectored Disease Seed Grant (124190-96210) and Foundation for Food and Agricultural Research New Innovator Award (2018-534299) to K.M.

Notes

The authors declare no competing financial interest.

■ ACKNOWLEDGMENTS

The authors would like to thank Denise Rossi and Ninfa Ramos (Texas A&M AgriLife Research) for the technical assistance in plant and insect propagation and Zhongliang Xing for assistance in gathering Raman spectra.

■ REFERENCES

(1) FoodData Central. Potatoes, flesh and skin, raw; FDC# 170026. https://fdc.nal.usda.gov/fdc-app.html#/food-details/170026/nutrients (accessed 2019-07-23) U.S. Department of Agriculture Agricultural Research Service.

(2) *Potato Statistical Yearbook 2018*; National Potato Council, 2018

(3) *Potatoes 2017 Summary*; United States Department of Agriculture, 2018.

(4) Kaur, L.; Singh, J. Chapter 21 - Novel Applications of Potatoes. In *Advances in Potato Chemistry and Technology*, Second Ed.; Singh, J., Kaur, L., Eds.; Academic Press: San Diego, CA, 2016; pp 627−649.

(5) Center for North American Studies, Economic Impacts of Zebra Chip on Texas; Texas A&M Agrilife Extension, 2009.

(6) Munyaneza, J. E. Zebra Chip Disease of Potato: Biology, Epidemiology, and Management. *Am. J. Potato Res.* **2012**, *89*, 329−350.

(7) Crosslin, J.; Lin, H.; Munyaneza, J. Detection of 'Candidatus Liberibacter Solanacearum'in the potato psyllid, Bactericera cockerelli

(Sulc) 1, by conventional and real-time PCR. *Southwest. Entomol.* **2011**, *36*, 125−136.
(8) Liefting, L. W.; Sutherland, P. W.; Ward, L. I.; Paice, K. L.; Weir, B. S.; Clover, G. R. A new 'Candidatus Liberibacter'species associated with diseases of solanaceous crops. *Plant Dis.* **2009**, *93*, 208−214.
(9) Li, W.; Abad, J. A.; French-Monar, R. D.; Rascoe, J.; Wen, A.; Gudmestad, N. C.; Secor, G. A.; Lee, I.-M.; Duan, Y.; Levy, L. Multiplex real-time PCR for detection, identification and quantification of 'Candidatus Liberibacter solanacearum' in potato plants with zebra chip. *J. Microbiol. Methods* **2009**, *78*, 59−65.
(10) Liang, P.-S.; Haff, R. P.; Hua, S.-S. T.; Munyaneza, J. E.; Mustafa, T.; Sarreal, S. B. L. Nondestructive detection of zebra chip disease in potatoes using near-infrared spectroscopy. *Biosystems Engineering* **2018**, *166*, 161−169.
(11) Gray, S.; De Boer, S.; Lorenzen, J.; Karasev, A.; Whitworth, J.; Nolte, P.; Singh, R.; Boucher, A.; Xu, H. Potato virus Y: an evolving concern for potato crops in the United States and Canada. *Plant Dis.* **2010**, *94*, 1384−1397.
(12) Karasev, A. V.; Gray, S. M. Continuous and Emerging Challenges of Potato virus Y in Potato. *Annu. Rev. Phytopathol.* **2013**, *51*, 571−586.
(13) Mehle, N.; Dobnik, D.; Ravnikar, M.; Pompe Novak, M. Validated reverse transcription droplet digital PCR serves as a higher order method for absolute quantification of Potato virus Y strains. *Anal. Bioanal. Chem.* **2018**, *410*, 3815−3825.
(14) Griffel, L. M.; Delparte, D.; Edwards, J. Using Support Vector Machines classification to differentiate spectral signatures of potato plants infected with Potato Virus Y. *Computers and Electronics in Agriculture* **2018**, *153*, 318−324.
(15) Couture, J. J.; Singh, A.; Charkowski, A. O.; Groves, R. L.; Gray, S. M.; Bethke, P. C.; Townsend, P. A. Integrating Spectroscopy with Potato Disease Management. *Plant Dis.* **2018**, *102*, 2233−2240.
(16) Antunes, V.; Serrão, V.; Candeias, A.; Mirão, J.; Cardoso, A.; Carvalho, M. L.; Fernandes, N.; Manso, M. Scrutinizing Ecce Homo: European or Indian painting? Assessment by Raman and complementary spectroscopic techniques. *J. Raman Spectrosc.* **2019**, *50*, 161−174.
(17) McLaughlin, G.; Fikiet, M. A.; Ando, M.; Hamaguchi, H.-o.; Lednev, I. K. Universal detection of body fluid traces in situ with Raman hyperspectroscopy for forensic purposes: Evaluation of a new detection algorithm (HAMAND) using semen samples. *J. Raman Spectrosc.* **2019**, *50*, 1147.
(18) Song, S. W.; Kim, J.; Eum, C.; Cho, Y.; Park, C. R.; Woo, Y.-A.; Kim, H. M.; Chung, H. Hyperspectral Raman Line Mapping as an Effective Tool To Monitor the Coating Thickness of Pharmaceutical Tablets. *Anal. Chem.* **2019**, *91*, 5810−5816.
(19) Egging, V.; Nguyen, J.; Kurouski, D. Detection and identification of fungal infections in intact wheat and sorghum hrain using a hand-held Raman spectrometer. *Anal. Chem.* **2018**, *90*, 8616−8621.
(20) Farber, C.; Kurouski, D. Detection and Identification of Plant Pathogens on Maize Kernels with a Hand-Held Raman Spectrometer. *Anal. Chem.* **2018**, *90*, 3009−3012.
(21) Farber, C.; Shires, M.; Ong, K.; Byrne, D.; Kurouski, D. Raman spectroscopy as an early detection tool for rose rosette infection. *Planta* **2019**, *250*, 1247−1254.
(22) Sanchez, L.; Ermolenkov, A.; Tang, X.-T.; Tamborindeguy, C.; Kurouski, D. Non-invasive diagnostics of Liberibacter disease on tomatoes using a hand-held Raman spectrometer. *Planta* **2020**, *251*, 64.
(23) Morey, R.; Ermolenkov, A.; Payne, W. Z.; Scheuring, D. C.; Koym, J. W.; Vales, M. I.; Kurouski, D. Non-invasive identification of potato varieties and prediction of the origin of tuber cultivation using spatially offset Raman spectroscopy. *Anal. Bioanal. Chem.* **2020**, *412*, 4585−4594.
(24) Sanchez, L.; Pant, S.; Xing, Z.; Mandadi, K.; Kurouski, D. Rapid and noninvasive diagnostics of Huanglongbing and nutrient deficits on citrus trees with a handheld Raman spectrometer. *Anal. Bioanal. Chem.* **2019**, *411*, 3125−3133.
(25) Sanchez, L.; Pant, S.; Mandadi, K.; Kurouski, D. Raman Spectroscopy vs Quantitative Polymerase Chain Reaction In Early Stage Huanglongbing Diagnostics. *Sci. Rep.* **2020**, *10*, 10101.
(26) Matousek, P.; Clark, I. P.; Draper, E. R. C.; Morris, M. D.; Goodship, A. E.; Everall, N.; Towrie, M.; Finney, W. F.; Parker, A. W. Subsurface Probing in Diffusely Scattering Media Using Spatially Offset Raman Spectroscopy. *Appl. Spectrosc.* **2005**, *59*, 393−400.
(27) Bloomfield, M.; Andrews, D.; Loeffen, P.; Tombling, C.; York, T.; Matousek, P. Non-invasive identification of incoming raw pharmaceutical materials using Spatially Offset Raman Spectroscopy. *J. Pharm. Biomed. Anal.* **2013**, *76*, 65−69.
(28) Matousek, P.; Stone, N. Development of deep subsurface Raman spectroscopy for medical diagnosis and disease monitoring. *Chem. Soc. Rev.* **2016**, *45*, 1794−1802.
(29) López-López, M.; García-Ruiz, C. Infrared and Raman spectroscopy techniques applied to identification of explosives. *TrAC, Trends Anal. Chem.* **2014**, *54*, 36−44.
(30) Jagoueix, S.; Bové, J. M.; Garnier, M. PCR detection of the two Candidatus liberobacter species associated with greening disease of citrus. *Mol. Cell. Probes* **1996**, *10*, 43−50.
(31) Chiong, K. T.; Damaj, M. B.; Padilla, C. S.; Avila, C. A.; Pant, S. R.; Mandadi, K. K.; Ramos, N. R.; Carvalho, D. V.; Mirkov, T. E. Reproducible genomic DNA preparation from diverse crop species for molecular genetic applications. *Plant Methods* **2017**, *13*, 106.
(32) Li, W.; Hartung, J. S.; Levy, L. Quantitative real-time PCR for detection and identification of Candidatus Liberibacter species associated with citrus huanglongbing. *J. Microbiol. Methods* **2006**, *66*, 104−115.
(33) Eriksson, L.; Johansson, E.; Kettaneh-Wold, N.; Trygg, J.; Wikström, C.; Wold, S. *Multi-and megavariate data analysis*; Umetrics Ab Umea: Sweden, 2006; Vol. *1*.
(34) Lee, L. C.; Liong, C.-Y.; Jemain, A. A. Partial least squares-discriminant analysis (PLS-DA) for classification of high-dimensional (HD) data: a review of contemporary practice strategies and knowledge gaps. *Analyst* **2018**, *143*, 3526−3539.
(35) Shashilov, V. A.; Lednev, I. K. Advanced statistical and numerical methods for spectroscopic characterization of protein structural evolution. *Chem. Rev.* **2010**, *110*, 5692−5713.
(36) van der Voet, H. Comparing the predictive accuracy of models using a simple randomization test. *Chemom. Intell. Lab. Syst.* **1994**, *25*, 313−323.
(37) Thomas, E. V. Non-parametric statistical methods for multivariate calibration model selection and comparison. *J. Chemom.* **2003**, *17*, 653−659.
(38) Chicco, D. Ten quick tips for machine learning in computational biology. *BioData Min.* **2017**, *10*, 35.
(39) Harrison, K.; Tamborindeguy, C.; Scheuring, D. C.; Herrera, A. M.; Silva, A.; Badillo-Vargas, I. E.; Miller, J. C.; Levy, J. G. Differences in Zebra Chip Severity between 'Candidatus Liberibacter Solanacearum' Haplotypes in Texas. *Am. J. Potato Res.* **2019**, *96*, 86−93.
(40) Almeida, M. R.; Alves, R. S.; Nascimbem, L. B.; Stephani, R.; Poppi, R. J.; de Oliveira, L. F. Determination of amylose content in starch using Raman spectroscopy and multivariate calibration analysis. *Anal. Bioanal. Chem.* **2010**, *397*, 2693−2701.
(41) Kizil, R.; Irudayaraj, J.; Seetharaman, K. Characterization of irradiated starches by using FT-Raman and FTIR spectroscopy. *J. Agric. Food Chem.* **2002**, *50*, 3912−3918.
(42) Edwards, H. G.; Farwell, D. W.; Webster, D. FT Raman microscopy of untreated natural plant fibres. *Spectrochim. Acta, Part A* **1997**, *53A*, 2383−2392.
(43) De Gussem, K.; Vandenabeele, P.; Verbeken, A.; Moens, L. Raman spectroscopic study of Lactarius spores (Russulales, Fungi). *Spectrochim. Acta, Part A* **2005**, *61*, 2896−2908.
(44) Schulz, H.; Baranska, M.; Baranski, R. Potential of NIR-FT-Raman spectroscopy in natural carotenoid analysis. *Biopolymers* **2005**, *77*, 212−221.
(45) Wiercigroch, E.; Szafraniec, E.; Czamara, K.; Pacia, M. Z.; Majzner, K.; Kochan, K.; Kaczor, A.; Baranska, M.; Malek, K. Raman

https://doi.org/10.1021/acsagscitech.1c00024
ACS Agric. Sci. Technol. 2021, 1, 211−221

and infrared spectroscopy of carbohydrates: A review. *Spectrochim. Acta, Part A* **2017**, *185*, 317−335.
(46) Zheng, R.; Zheng, X.; Dong, J.; Carey, P. R. Proteins can convert to beta-sheet in single crystals. *Protein Sci.* **2004**, *13*, 1288−1294.
(47) Larsen, K. L.; Barsberg, S. Theoretical and Raman Spectroscopic Studies of Phenolic Lignin Model Monomers. *J. Phys. Chem. B* **2010**, *114*, 8009−8021.
(48) Cael, J. J.; Koenig, J. L.; Blackwell, J. Infrared and raman spectroscopy of carbohydrates. Part 4: Normal coordinate analysis of V-amylose. *Biopolymers* **1975**, *14*, 1885−1903.
(49) Adar, F. Carotenoids—Their Resonance Raman Spectra and How They Can Be Helpful in Characterizing a Number of Biological Systems. *Spectroscopy* **2017**, *32*, 12−20.
(50) Agarwal, U. P. Raman imaging to investigate ultrastructure and composition of plant cell walls: distribution of lignin and cellulose in black spruce wood (Picea mariana). *Planta* **2006**, *224*, 1141−1153.
(51) Kang, L.; Wang, K.; Li, X.; Zou, B. High pressure structural investigation of benzoic acid: raman spectroscopy and X-ray diffraction. *J. Phys. Chem. C* **2016**, *120*, 14758−14766.
(52) Pompeu, D. R.; Larondelle, Y.; Rogez, H.; Abbas, O.; Pierna, J. A. F.; Baeten, V. Characterization and discrimination of phenolic compounds using Fourier transformation Raman spectroscopy and chemometric tools. *Biotechnol. Agron. Soc. Environ.* **2017**, *22*, 1−16.
(53) Gold, K. M.; Townsend, P. A.; Herrmann, I.; Gevens, A. J. Investigating potato late blight physiological differences across potato cultivars with spectroscopy and machine learning. *Plant Sci.* **2020**, *295*, 110316.
(54) Buchman, J. L.; Fisher, T. W.; Sengoda, V. G.; Munyaneza, J. E. Zebra Chip Progression: From Inoculation of Potato Plants with Liberibacter to Development of Disease Symptoms in Tubers. *Am. J. Potato Res.* **2012**, *89*, 159−168.
(55) Lachman, J.; Hamouz, K.; Orsák, M.; Kotíková, Z. Carotenoids in potatoes−a short overview. *Plant, Soil Environ.* **2016**, *62*, 474−481.
(56) Bernards, M. A.; Razem, F. A. The poly(phenolic) domain of potato suberin: a non-lignin cell wall bio-polymer. *Phytochemistry* **2001**, *57*, 1115−1122.
(57) Vogt, T. Phenylpropanoid biosynthesis. *Mol. Plant* **2010**, *3*, 2−20.
(58) Singh, R. K.; Navarre, D. A.; Brown, C. R. Relationship between Sugars and Phenylpropanoids in Tubers from Diverse Genotypes. *Am. J. Potato Res.* **2016**, *93*, 581−589.
(59) Gumul, D.; Ziobro, R.; Noga, M.; Sabat, R. Characterisation of five potato cultivars according to their nutritional and pro-health components. *Acta Sci. Pol., Technol. Aliment.* **2011**, *10*, 77−81.
(60) Graça, J. Suberin: the biopolyester at the frontier of plants. *Front. Chem.* **2015**, *3*, 62.
(61) Almeida, M. R.; Alves, R. S.; Nascimbem, L. B.; Stephani, R.; Poppi, R. J.; de Oliveira, L. F. Determination of amylose content in starch using Raman spectroscopy and multivariate calibration analysis. *Anal. Bioanal. Chem.* **2010**, *397*, 2693−2701.
(62) Kizil, R.; Irudayaraj, J.; Seetharaman, K. Characterization of irradiated starches by using FT-Raman and FTIR spectroscopy. *J. Agric. Food Chem.* **2002**, *50*, 3912−3918.
(63) Edwards, H. G.; Farwell, D. W.; Webster, D. FT Raman microscopy of untreated natural plant fibres. *Spectrochim. Acta, Part A* **1997**, *53A*, 2383−2392.
(64) De Gussem, K.; Vandenabeele, P.; Verbeken, A.; Moens, L. Raman spectroscopic study of Lactarius spores (Russulales, Fungi). *Spectrochim. Acta, Part A* **2005**, *61*, 2896−2908.
(65) Wiercigroch, E.; Szafraniec, E.; Czamara, K.; Pacia, M. Z.; Majzner, K.; Kochan, K.; Kaczor, A.; Baranska, M.; Malek, K. Raman and infrared spectroscopy of carbohydrates: A review. *Spectrochim. Acta, Part A* **2017**, *185*, 317−335.
(66) Zheng, R.; Zheng, X.; Dong, J.; Carey, P. R. Proteins can convert to beta-sheet in single crystals. *Protein Sci.* **2004**, *13*, 1288−1294.
(67) Larsen, K. L.; Barsberg, S. Theoretical and Raman Spectroscopic Studies of Phenolic Lignin Model Monomers. *J. Phys. Chem. B* **2010**, *114*, 8009−8021.
(68) Kang, L.; Wang, K.; Li, X.; Zou, B. High pressure structural investigation of benzoic acid: raman spectroscopy and x-ray diffraction. *J. Phys. Chem. C* **2016**, *120*, 14758−14766.

https://doi.org/10.1021/acsagscitech.1c00024
ACS Agric. Sci. Technol. 2021, 1, 211−221